Iron topochemistry and surface reactivity of amphibole asbestos: Relations with in vitro toxicity

ARTICLE *in* ANALYTICAL AND BIOANALYTICAL CHEMISTRY · NOVEMBER 2011

Impact Factor: 3.44 · DOI: 10.1007/s00216-011-5525-y · Source: PubMed

8 AUTHORS, INCLUDING:

Giovanni B Andreozzi
Sapienza University of Rome
81 PUBLICATIONS **694** CITATIONS
SEE PROFILE

Lorenzo Stievano
Université de Montpellier, Montpellier, France
130 PUBLICATIONS **1,629** CITATIONS
SEE PROFILE

Guendalina Lucarini
Università Politecnica delle Marche
117 PUBLICATIONS **1,688** CITATIONS
SEE PROFILE

Maria Rita Rippo
Università Politecnica delle Marche
42 PUBLICATIONS **2,187** CITATIONS
SEE PROFILE

Anal Bioanal Chem (2012) 402:871–881
DOI 10.1007/s00216-011-5525-y

ORIGINAL PAPER

Iron topochemistry and surface reactivity of amphibole asbestos: relations with in vitro toxicity

Alessandro Pacella · Giovanni B. Andreozzi · Jeanine Fournier · Lorenzo Stievano · Federica Giantomassi · Guendalina Lucarini · Maria Rita Rippo · Armanda Pugnaloni

Received: 30 August 2011 / Revised: 17 October 2011 / Accepted: 19 October 2011 / Published online: 6 November 2011

Abstract Chemical reactivity of asbestos tremolite from Italy and USA localities and Union Internationale Contre le Cancer (UICC) crocidolite was studied in relation to Fe content, oxidation state, and structural coordination. Direct correlation between amount of Fe^{2+} at the exposed M(1) and M(2) sites of the amphibole structure and fiber chemical reactivity was established. The in vitro toxicity of the same samples was investigated on human alveolar A549 cell line. Relationship between crystal-chemical features and cell toxicity is not straightforward. UICC crocidolite has Fe content and chemical reactivity largely higher than that of tremolite samples, but all show comparable in vitro toxic potential. Results obtained evidenced that Fe topochemistry is not a primary factor for induced cell toxicity, though it accounts for asbestos chemical reactivity (and possibly genotoxicity).

A. Pacella (✉) · G. B. Andreozzi
Dipartimento di Scienze della Terra, Sapienza Università di Roma,
Piazzale Aldo Moro 5,
00185, Rome, Italy
e-mail: alessandro.pacella@uniroma1.it

J. Fournier · L. Stievano
UPMC Paris VI, UMR 7197, Laboratoire de Réactivité de Surface,
"Le St Raphaël", 3, rue Galilée, Ivry-Sur-Seine,
94200, Paris, France

L. Stievano
Institut Charles Gerhardt-AIME, UMR CNRS 5253,
Université Montpellier 2,
34095, Montpellier, France

F. Giantomassi · G. Lucarini · M. R. Rippo · A. Pugnaloni
Dipartimento di Scienze Cliniche e Molecolari,
Universita' Politecnica delle Marche,
via Tronto n10/A,
60020, Torrette (Ancona), Italy

Keywords Asbestos amphiboles · Fe topochemistry · Surface reactivity · Lipid peroxidation · In vitro toxicity

Introduction

Asbestos fibers are undoubtedly related to various respiratory diseases: *asbestosis*, a non-malignant diffuse interstitial fibrosis of the lung tissue; *lung cancers*, particularly bronchogenic carcinomas including squamous cell carcinomas, small- and large-cell carcinoma, and adenocarcinomas; *mesothelioma*, a cancer mainly developing in the pleura and also in the peritoneum and the pericardium. The main features of such tumors are: long latency (up to 20 or 30 years after asbestos exposure), difficult diagnosis, and ability to appear even after the inhalation of an extremely low asbestos concentration [1]. Epidemiological data showed that moderate exposure to chrysotile (serpentine asbestos) presents a very low health risk compared with amphibole asbestos. This seems to be linked to the largely different solubility of asbestos fibers in the biological medium: very high for chrysotile and significantly lower for amphibole asbestos [2, 3].

The mechanism through which asbestos give rise to respiratory diseases has not been completely clarified so far. The toxic action of reactive oxygen species (ROS) is considered as the common key in these types of pathologies. In fact, ROS may damage all cellular biomolecules, including lipids, proteins, carbohydrates, and nucleic acids, and play an important role in asbestos-induced cytotoxicity and genotoxicity [4–8]. Notably, ROS production is mainly due to endogenous factors since they are continuously formed in several metabolic processes as oxidative stress [9–11]. In addition to endogenous factors, exogenous pathogenic factors can also enhance cellular ROS produc-

tion and, among these, mineral fibers may be markedly relevant [12–14]. In particular, the presence and structural coordination of Fe in the mineral fibers were proposed to be important factors in the generation of ROS [11, 15–18]. Among the different ROS, it is necessary to distinguish between those with strong electrophilic character (metal oxo species, hydroxyl radicals, etc.), able to attack a great variety of target molecules, and those with weak electrophilic character (iron super-oxo species, various oxygenated complexes of Fe^{3+}, etc.), only able to trigger lipid peroxidation [14, 19, 20]. The hydroxyl radical (HO·) is one of the strongest electrophilic ROS and is investigated in most reactivity studies. The production of HO· implies an interaction of iron-containing materials with an oxygen target such as molecular oxygen or hydrogen peroxide H_2O_2, according to the Fenton reaction or Haber–Weiss cycle [15].

The relationships between asbestos exposure and associated diseases became clearly known around 1960 [21] and are based mainly on investigations carried out in workplaces. However, the presence of asbestos in the air may be also related to environmental causes, e.g., the widespread diffusion of asbestos-bearing rocks. For example, recent epidemiological studies showed the presence of asbestos-related pathologies in small villages in Turkey, Greece, Cyprus, Corsica, and New Caledonia [22]. Population of these localities, which lie within or near to ophiolite complexes, has been exposed to asbestos (in particular, tremolite and actinolite asbestos) quarried from local rocks and used as an ingredient for stucco and whitewash [22]. Ophiolite complexes are fragments of oceanic lithosphere obducted onto the edges of continental plates, and have exceptional physical and mechanical qualities such as strength, durability, variety in appearance, and color. Such qualities determine their large use as building and ornamental stones. Ophiolitic complexes hosting fibrous tremolite and actinolite have been observed in some areas of the USA as Virginia, Maryland, Pennsylvania, and California (El Dorado County) [22]. Due to the possible health risks that the mineral dust might have on the local residents, an asbestos exposure control plan has been instituted [22]. In Italian localities of the Western Alps and the Apennines, ophiolitic outcrops hosting chrysotile, tremolite–actinolite, and anthophylite asbestos are also abundant. In the Susa Valley (Piedmont, NW Italy), high environmental hazard was recognized in relation to recent excavations for railway tunnels through metamorphic formations, such as serpentinites which contain tremolite fibers [23]. As a matter of fact, fibers of tremolite from the ophiolitic outcrops of Ala di Stura (Lanzo Valley, Piedmont) showed high carcinogenicity and very long incubation time as a result of in vivo experiments [24–26]. Ophiolites hosting fibrous tremolite also outcrop in the regions of Latium [27] and Calabria [28], where quarries of such materials have been widely used in the past. Moreover, fibrous tremolite is present in the soils of Lauria and Castelluccio Superiore Towns (Potenza), where pleural mesothelioma cases were observed [29].

In this work we have investigated the harmful potential of fibrous tremolite samples coming from Italy and USA, previously carefully characterized. As positive reference, a sample of Union Internationale Contre le Cancer (UICC, Johannesburg, South Africa) crocidolite was analyzed. Chemical reactivity of the fibrous samples was studied on the basis of Fe crystal chemistry (i.e., Fe amount, oxidation state, and structural coordination); possible relations with in vitro toxicity on human alveolar A549 cell line were tentatively investigated.

Experimental

Materials

The samples studied in this work are fibrous tremolites coming from different ophiolitic outcrops of Italy, from north to south: Ala di Stura (Lanzo Valley, Piedmont), Mt. Rufeno (Acquapendente, Latium), and Castelluccio Superiore (Potenza, Basilicata). In addition, one American tremolite coming from the ophiolite complex outcropping in Maryland (Montgomery County) was studied. Moreover, a sample of UICC crocidolite, well known to be highly harmful, was analyzed for comparison.

The detailed crystal-chemical characterization of tremolite samples has been previously carried out by Pacella et al. [30] by combining inductively coupled plasma-mass spectrometry, electron microprobe analysis, scanning electron microscopy with microanalysis system, parallel-beam X-ray powder diffraction, ^{57}Fe Mössbauer spectroscopy, and Fourier-transform infrared spectroscopy.

Surface reactivity studies

HO· radical production

The capability of the fibrous samples to release free radicals was evaluated by measuring the HO· radical production in the presence of H_2O_2 via Fenton reaction. All tests were performed in a reactor at 37 °C, in the absence of light. The reaction mixture contained 25 mg of sample (previously ground for 1 min), 0.5 ml of sodium phosphate buffer (Na_2HPO_4–NaH_2PO_4; 99% in purity, Sigma) at pH=7.4 (0.5 M), 1 ml of aqueous buffered solution of 5.5-dimethyl-1-pyrroline-*N*-oxide (DMPO, Aldrich, 97% in purity) as a radical trapping agent (0.1 M), and 0.5 ml of buffered H_2O_2 (0.6 vol.%) obtained after dilution of commercial diluition

(Prolabo, Normapur). The reactor was placed on a swinging table in order to ensure the homogeneity of the suspension. After 5 and 30 min of incubation time, fractions of the suspension were filtered (cellulose acetate filter, 0.22 μm) and the filtrate was transferred to a flat quartz cell for the detection of the radical adduct [DMPO, HO]° by electron paramagnetic resonance (EPR) spectroscopy. Control measurements were realized in parallel using blank solutions not containing fibrous samples under the same experimental conditions.

The EPR spectra of [DMPO, HO]° were obtained at room temperature using a Brucker ESP-300E spectrometer. Analytical conditions were: magnetic field, 3,440 G; frequency field, 9.65 GHz; power, 10 mW; frequency modulation, 100 KHz; modulation amplitude, 3.24 G and gain of $5*10^4$; and acquisition time, 84.92 ms.

Lipid peroxidation

Lipid peroxidation was investigated by measuring the formation of malonaldehyde (MDA) and two classes of monoaldehydes (saturated and unsaturated monoaldehydes) produced by the degradation of linolenic acid (polyunsaturated fatty acid) in presence of the fibrous samples. All tests were performed in aerated sodium phosphate buffer (Na_2HPO_4–NaH_2PO_4; 99% in purity, Sigma) at pH 7.4 (0.5 M). The sample (25 mg) was ground in an agate mortar for 1 min and then placed in a reactor with 0.5 ml of H_2O_2 (0.3 vol.%) and 0.5 ml of a previously purified linolenic acid or 9,12,15-octadecatrienoic acid (99% in purity, Sigma) solution. The reactor was placed on a swinging table in order to ensure the homogeneity of the suspension. Control measurements were realized in parallel using blank solutions not containing fibrous samples under the same experimental conditions. After an incubation time of 18 h, 100 μL of butylated hydroxytoluene (BHT; 99.5% in purity, Sigma) solution (0.20.2 wt.% in ethanol) were added to the suspension in order to stop the peroxidation process of the fatty acid. After BHT addition, 2 ml of a TBA reagent containing 0.375% (*w*/*v*) of TBA (98% in purity, Sigma) and 15% (*w*/*v*) of trichloroacetic acid (99.5% in purity, Merck) in HCl 0.25 M [31] were added to the mixture. Subsequently, the solution was incubated for 15 min in water bath at 100 °C. After cooling to room temperature, 3 mL of 1-butanol (99.5% in purity, Merck) were added, and the solution was centrifuged for 10 min (8,000 rpm), in order to extract the pink and yellow chromogens formed (TBA-MDA-TBA and TBA-monoaldehyde, respectively). The upper phase (butanol) containing colored chromogens was measured at λ=535 nm for TBA-MDA-TBA, λ=500 nm for TBA-saturated monoaldehyde, and λ=450 nm for TBA-polyunsaturated monoaldehyde [20, 32] against the pure 1-butanol as a reference by UV-visible spectrometer (Jasco, V-550).

In vitro tests

Biological effects of the fibrous samples were tested in vitro on A549 cell lines (American Type Culture Collection, Rockville, MD, USA, number CCL-185). A549 cell line is currently used as a model to study cell proliferation, cell motility and cytotoxicity exerted by different asbestos fibers on human alveolar epithelial cells [33, 34]. They mimic cell-fiber interactions in lung type II epithelium as they internalize asbestos fibers soon after exposure. The cells were grown in controlled atmosphere in RPMI-1640 (Gibco, USA) supplemented with 10% FBS (Gibco, USA), 2 mM l-glutamine, 100 U/ml penicillin, and 100 U/ml streptomycin (Sigma-Aldrich, Milan, Italy). Cells were passaged every 1–3 days by digestion with 0.25% trypsin (Sigma-Aldrich, Milan, Italy, containing 0.02% EDTA). After 24 h the spent culture medium was replaced with fresh medium. Fibrous samples were added to the cell cultures at concentration of 50 μg/ml and cells were then incubated for 24 and 48 h.

MTT assay

The cytotoxic action induced by the different fibrous samples was evaluated by 3-(4,5-dimethylthiazol-2-yl)-2,5-diphenyltetrazolium bromide (MTT) assay [35]. This test provides an appropriate technique to measure cell viability decrements. For MTT assay A549 cells were seeded at a density of 3×10^4 cells/well into 24-well microplates in three replicates. After treatment, the medium was removed and 200 μl MTT solution (Sigma, St. Louis, USA. 5 mg/ml in RPM1-1640) and 1.8 ml RPM1-1640 were added to cells. The multiwell plates were then incubated at 37 °C for 3 h. After discarding supernatants, the formazan crystals were dissolved in 2 ml of solvent (4% HCl, 1 M in absolute isopropanol). The amount of formazan crystals is directly related to the number of viable cells. The optical density was measured at 570 nm (reference filter, 690 nm) using a spectrofluorimeter (Secomamam Anthelie light version 3.8, Contardi, Italy). Data were expressed as relative cell viability using the following equation: relative viability (%) = Absorbance (Treatment)/ Absorbance (Vehicle Control)×100. Control monolayers were grown in culture medium with no treatments; their absorbance values were taken as reference values and considered as 100% of cell viability. Data obtained from three assays are expressed as mean values± standard deviation. Statistical evaluations were done using the *t* test with Bonferroni's correction for multiple comparisons ($p<0.05$).

Ki-67 assay

The study of rates changes of cell cycle perturbation and cell proliferation is considered an useful tool to evaluate the toxic effect of asbestos minerals. A strong correlation between cell proliferative activity (*S*-phase fraction) and Ki-67 index has been demonstrated [36, 37]. On this basis, quantitative assessment of Ki-67 protein provides an accurate estimate of the proliferation index [38, 39]. For detection of Ki-67 protein cells were seeded at a density of 3×10^4 cells/slide on two glass slides and treated with minerals at the concentration of 50 μg/ml 24 h after seeding to improve adhesion to the substrate. Monolayers were fixed in cold acetone for 10 min, permeabilized in 0.5% Triton X-100 (Sigma-Aldrich, Italy) in phosphate-buffered saline (PBS) for 10 min and then incubated overnight at 4 °C with the MIB-1 mouse monoclonal antibody (pre-diluted, Dakocytomation, Dako, Carpinteria, USA). The reaction was revealed using the streptoavidin-biotin peroxidase technique (Dako Envision Plus/HRP peroxidase kit, Dakocytomation, Dako, Carpinteria, USA). Section were incubated with 3.3′ diaminobenzidine in 0.05 M Tris buffer (pH 7.6) with 0.01% hydrogen peroxide. Slides were rinsed in running tap water for 10 minutes, counterstained with Mayer's haematoxylin (Bio-Optica SPA, Milano, Italy), dehydrated in ethanol and cover-slipped with Eukitt mounting medium (Electron Microscopy Sciences, Hatfield, PA). Positive controls were obtained from sections of breast carcinoma. Negative controls were performed by substituting the primary antibody with non immune serum. The immunolocalization of MIB-1 was evaluated by morphometric investigations with light microscopy (Nikon Eclipse E 600). Immunopositive cells were observed in ten fields at ×200 magnification. The number of MIB-1 immunopositive cells was expressed as a percentage of the total counted cells. Data obtained from three assays are expressed as mean values±standard deviation. Statistical evaluations were performed using the *t* test with Bonferroni's correction for multiple comparisons ($p<0.05$).

Analysis of pycnotic nuclei by fluorescence microscopy

Nuclear pycnosis, i.e., shrinkage and clumping of genetic material into a dense mass, and the degraded DNA of apoptotic cells resulting in hypodiploid DNA content are evidences of cellular stress [40]. Therefore, in this work fibers-induced toxicity was also studied by the evaluation of pycnotic and hypodiploid nuclei.

For the analysis of pycnotic nuclei, A549 cells were seeded onto two glass slides at a density of 3×10^4 cells/cm^2 in RPMI-1640. Aderent cells were treated with 50 μg/ml of sample for 24 or 48 h. At the end of the treatment cells were washed in PBS, fixed in 4% formaldehyde in PBS for 5 min at room temperature (RT) and permeabilized in PBS/0.1% Triton X-100 for 10 min. After three washes in PBS at RT, a TRITC phalloidin solution (1:50 dilution in PBS, Sigma) was added for 40 min at RT. Samples were then washed and counterstained with Hoechst 33342 buffer solution (1:10,000 in PBS) for 15 min, washed again and analyzed using an Eclipse E600 fluorescence microscope (Nikon, Italia) at ×400 magnification. Untreated A549 cells cultured for 24 or 48 h were used as control.

Evaluation of hypodiploid nuclei was obtained by fluorescence activated cell scanning (FACS) analysis. Cells were treated with the fibers for 96 h; in order to evaluate apoptosis both floating and attached cells were pooled and stained with propidium iodide (PI), a DNA intercalating agent and a fluorescentz molecule. In particular, floating cells from the surnatant and adherent cells harvested in the appropriate manner were collected and fixed in ethanol 70 % in PBS for 30 min at 4 °C. After 2 washes in PBS the specimens were stained with propidium iodide (50 ug/ml) and 10 mg/ml RNase. Hypodiploid nuclei of apoptotic cells were analyzed by flow cytometry (Becton Dickinson FACS, San Diego, CA). A pass filter of 585 nm was used to collect PI fluorescence, acquiring 10000 events for each event. The percentage of the elements in the G1, S and G2 cycle phases was also evaluated. Untreated A549 cells were used as control.

Morphological and ultrastructural investigations

Morphological and ultrastructural investigations were performed to examine structural cell injuries and processed to preserve the cell contacts as monolayers. Cells were treated with 50 μg/ml of sample (Castelluccio Superiore and Ala di Stura tremolite) for incubation time of 24 and 48 h. Untreated cells were used as a control culture. After incubation, monolayers were fixed in 1.5 % (*v*/*v*) glutaraldehyde in 0.1 M cacodylate buffer (pH 7.4) for 30 min at 37 °C, washed in three changes of sodium cacodylate buffer, 5 min each, treated with 0.25% trypsin EDTA for 10 min at 37 °C, and detached. Suspensions were centrifuged and post-fixed in 1% osmium tetraoxide in 0.1 M cacodylate buffer for 1 h at 4 °C, suspended in 70% agarose (GellyPhorLE, Euroclone, Milano, Italy) and dehydrated in a graded alcohol series (70%, 95%, and 100%). Cells were processed through propylene oxide, embedded in araldite resin (Sigma) and polymerized at 60 °C for 48 h. Ultrathin sections were cut with an ultramicrotome LKB NOVA, placed on copper / rhodium grids and stained with 1% (*w*/*v*) uranyl acetate and lead citrate. Morphological and ultrastructural investigations were performed with a transmission electron microscope (TEM) CM 10 (Philips; Eindhoven, the Netherlands) operating at 80 kV.

Results and discussion

Crystal chemistry and surface chemistry of fibrous samples

Results obtained on the Italian tremolites showed that they have distinct but relatively small Fe content (Castelluccio Superiore<Mt. Rufeno<Ala di Stura). Notably, the sample from Maryland has Fe content almost double than the Italian ones [30]. Site population was assigned by combining chemical, spectroscopic and structural (Rietveld refinement) data, and the following crystal-chemical formulae were obtained:

Castelluccio Superiore

$$^{B}(Ca_{1.87}Na_{0.06}K_{0.01}Mn_{0.01}Mg_{0.05})_{\Sigma 2.00}\,^{C}(Mg_{4.79}Fe^{2+}_{0.19}Mn_{0.01}Fe^{3+}_{0.05}\,^{VI}Al_{0.01})_{\Sigma 5.06}\,^{T}(Si_{7.99}Al_{0.01})_{\Sigma 8.00}O_{22}\,^{O(3)}(OH_{1.97}F_{0.02})_{\Sigma 1.99}$$

Mt. Rufeno

$$^{B}(Ca_{1.84}Na_{0.10}Mn_{0.01})_{\Sigma 1.95}\,^{C}(Mg_{4.64}Fe^{2+}_{0.20}Mn_{0.01}Fe^{3+}_{0.06}\,^{VI}Al_{0.08})_{\Sigma 5.02}\,^{T}(Si_{7.99}Al_{0.01})_{\Sigma 8.00}O_{22}\,^{O(3)}(OH_{1.97}F_{0.03})_{\Sigma 2.00}$$

Ala di Stura

$$^{B}(Ca_{1.96}Na_{0.02})_{\Sigma 1.98}\,^{C}(Mg_{4.69}Fe^{2+}_{0.25}Mn_{0.03}Fe^{3+}_{0.03})_{\Sigma 5.00}\,^{T}(Si_{7.99}Al_{0.01})_{\Sigma 8.00}O_{22}\,^{O(3)}(OH_{1.98}F_{0.02})_{\Sigma 2.00}$$

Maryland

$$^{B}(Ca_{1.99}Na_{0.01}Mn_{0.02})_{\Sigma 2.02}\,^{C}(Mg_{4.48}Fe^{2+}_{0.44}Mn_{0.02}Fe^{3+}_{0.08})_{\Sigma 5.02}\,^{T}(Si_{7.95}Al_{0.01})_{\Sigma 7.96}O_{22}\,^{O(3)}(OH_{1.97}F_{0.01})_{\Sigma 1.98}$$

with B, C, T, and O(3) groups filled according to the order recommended by Leake et al. [41].

The crystal-chemical formula retrieved for the reference UICC crocidolite resulted to be consistent with that

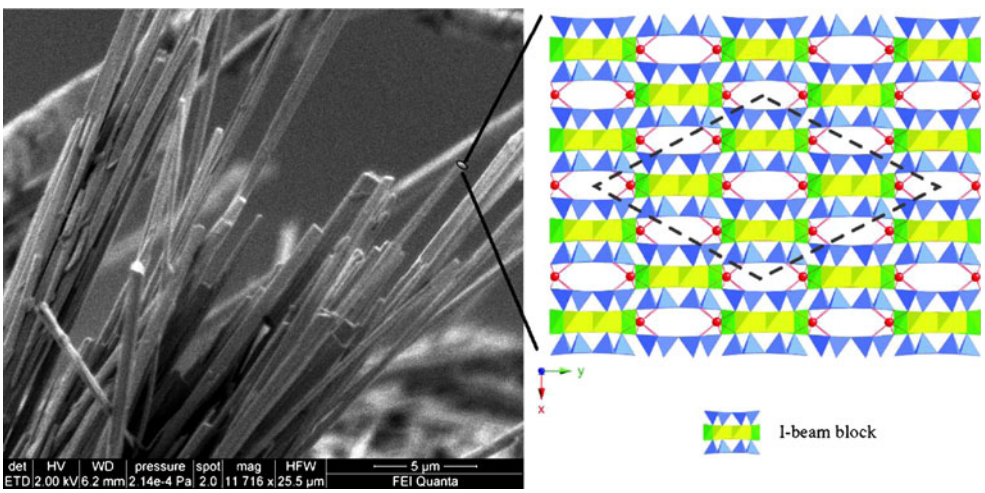

Fig. 1 *Left side*, SEM image of tremolite fibers from Castelluccio Superiore showing the prismatic, elongated, parallel fibers tightly packed, and randomly oriented around a common *c*-axis. *Right side*, tremolite structure projected along *c*-axis. *Blue tetrahedra*=T(1) and T(2); *yellow octahedra*=M(1); *green octahedra*=M(2); and *red dots*=M(4). *Dashed lines* embody the ideal {110} amphibole cross-section

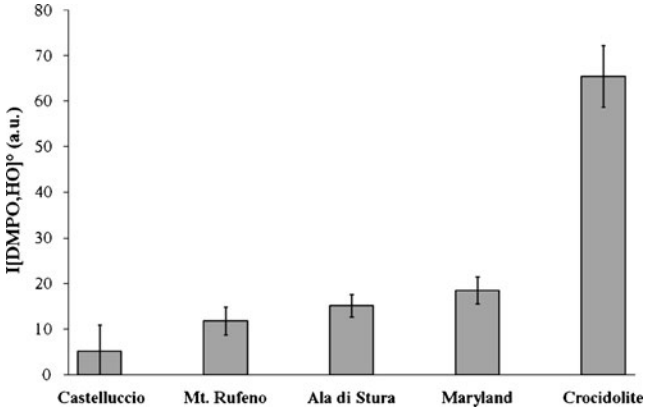

Fig. 2 Intensity of the [DMPO, HO]° radical adduct obtained from the tested samples. Mean values of two measurements, ±2 SD. Amphibole fibrous samples are ranked based on increasing Fe content

reported by Bowes and Farrow [42] and very close to that of the ideal crocidolite (that is the mineral riebeckite, $^{B}Na_2{}^{C}(Fe^{2+}{}_3Fe^{3+}{}_2)_{\Sigma 5}{}^{T}Si_8O_{22}{}^{O(3)}(OH)_2$). UICC crocidolite, the Fe-richest sample, has Fe^{2+} equally distributed over M(1) and M(3) sites, filling them almost completely. In addition, Fe^{3+} totally fills M(2) sites and the residuals fill M(1) and M(3) sites. On the contrary tremolite samples, which contain Fe ten times less than crocidolite, have Fe^{2+} equally distributed over M(1), M(2), and M(3) sites, and Fe^{3+} only allocated at M(2) sites.

Both the site occupation and the coordination environment of Fe in the structure play a central role in the interaction between fibers and biological environment, being only the Fe exposed at the surface involved in biochemical reactions [9, 17, 43]. Structure of both tremolite and crocidolite is monoclinic (*C*2/*m*) and consists of double chains of tetrahedra (T(1) and T(2)) aligned along the *c*-axis, and a strip of octahedra (M(1), M(2), and M(3), corresponding to C group) at the center of structural "I-beam" blocks. The I-beam blocks extend in *c* direction and are linked by M(4) distorted polyhedra, corresponding to B group. Moreover, it was reported that the amphibole fibers are composed of smaller, parallel fibrils tightly packed and randomly oriented around a common elongation *c*-axis [44, 45]. On these bases, we may consider each fibril as made of a number of I-beam blocks, exhibiting M(1), M(2), and M(4) sites on external surfaces (Fig. 1). Therefore, Fe^{2+} at M(1) and M(2) sites has higher probability of being involved in surface reactions than Fe^{2+} at M(3) site. Notably, in UICC crocidolite Fe^{2+} content at M(1) is ca. 2 atoms per formula unit (apfu) and Fe^{3+} content at M(2) sites is ca. 2 apfu, that is up to twenty times with respect to tremolite samples [30].

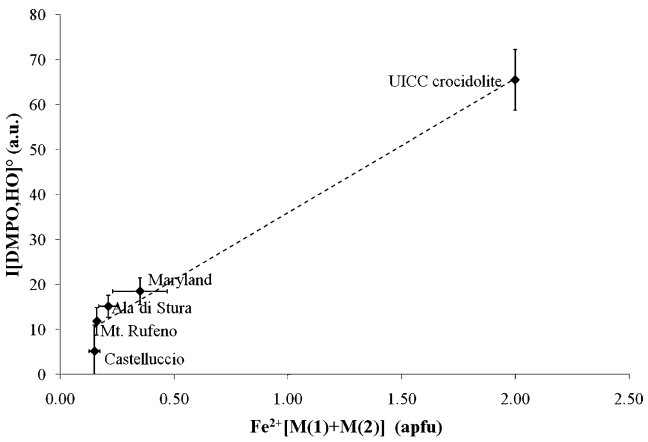

Fig. 3 Intensity of the [DMPO,HO]° radical adduct obtained from the tested samples as a function of their $^{[M(1)+M(2)]}Fe2+$ content. *Error bars*, ±2 SD

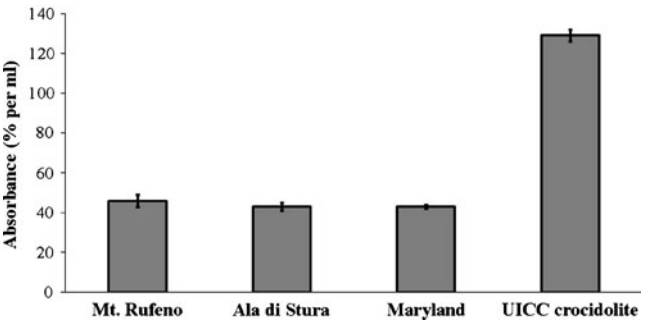

Fig. 4 Formation of MDA (% absorbance per milliliter of organic phase) observed for the tested samples. Mean values of two measurements, ±2 SD. Amphibole fibrous samples are ranked based on increasing Fe content

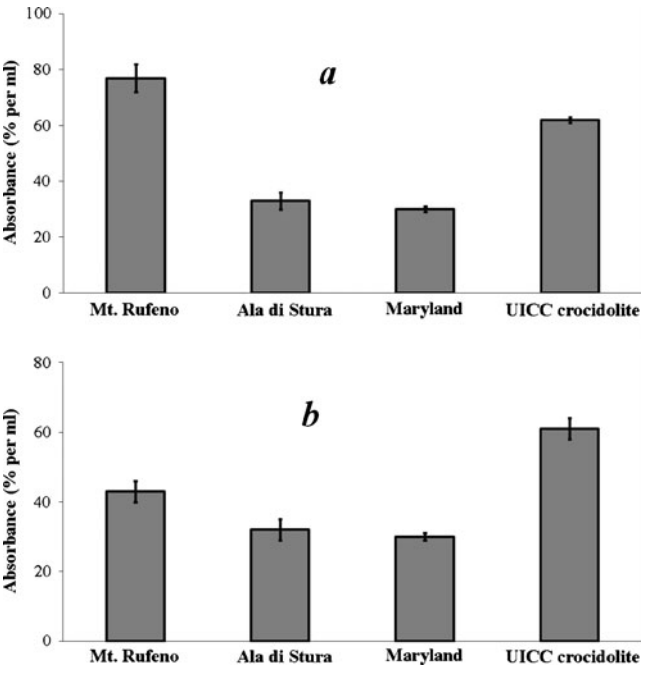

Fig. 5 Formation of monoaldehydes (% absorbance per ml of organic phase) observed for the tested samples: (**a**) polyunsaturated monoaldehydes at 450 nm; (**b**) saturated monoaldehydes at 500 nm. Mean values of two measurements, ±2 SD. Amphibole fibrous samples are ranked based on increasing Fe content

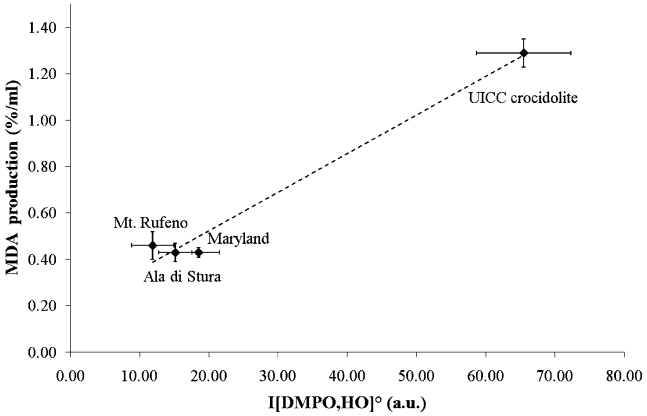

Fig. 6 MDA production of the tested samples as a function of HO· radical production. *Error bars*, ±2 SD

Surface reactivity of fibrous samples

Surface reactivity evaluated by production of (DMPO, HO)° radicals was measured by EPR and is reported as the average of the signal collected after 5 and 30 min of incubation time, subtracted by the value obtained for the control. Production of HO· radicals by UICC crocidolite is much higher than that of tremolite samples, and the reactivity of Maryland tremolite is slightly higher than that of the Italian ones (Fig. 2). Notably, the observed production of HO· radicals correlates well with the Fe^{2+} content at M(1) and M(2) sites (Fig. 3), comforting the hypothesis that the Fe^{2+} at M(1) and M(2) sites is the most reactive species. Maryland tremolite and UICC crocidolite were previously studied by XPS, and the oxidation state for Fe at the fiber surface was obtained: results revealed that their surface is enriched in Fe^{3+} with respect to the bulk, and this Fe^{3+} is mainly present as iron oxyhydroxides species [46]. The oxidation of Fe^{2+} to Fe^{3+} on the surface of the fibers is expected to inhibit, or at least delay their reactivity [9, 47, 48].

Surface reactivity evaluated through lipid peroxidation is reported as the average value derived from duplicate tests and is expressed as absorbance per milliliter of organic phase, subtracted by the value obtained for the control. Data referred to Castelluccio tremolite are not available since the available amount of this sample was insufficient to allow its analysis. The presence of MDA and monoaldehydes observed in the organic phase indicates that all the studied samples are active in the peroxidation process (Figs. 4 and 5). UICC crocidolite exhibits the highest reactivity in the formation of MDA; tremolite samples show comparable behavior among them but markedly lower reactivity (Fig. 4). Notably, among the various products generated by the lipid peroxidation, MDA is the most mutagenic and carcinogenic [49, 50]. Less systematic results are obtained when considering the production of monoaldehydes and kind of correlation is absent, with Mt. Rufeno sample resulting as highly reactive as UICC crocidolite (Fig. 5). This problematic result poses difficult-to-answer questions. Previous studies have implicated the presence of ROS as the agent inducing the lipid peroxidation [11, 19, 51]. Our data partially support such hypothesis, because they show that the MDA formation increases with the production of HO· radicals, which is one of the strongest electrophilic ROS (Fig. 6). However, no correlation could be found between the production of HO· radical and the generation of monoaldehydes, so the problem is still open. It is worth noting that, in addition to ROS with strong electrophilic character (HO·, iron-oxo species) which are able to attack a great variety of molecules (such as DNA), other less electrophilic species (iron super-oxo, iron-peroxo, etc.) are also capable to trigger lipid peroxidation [52]. Further investigation in this direction is in progress at the moment.

In vitro toxicity of fibrous samples

TEM images of human alveolar epithelial A549 control cells grown in monolayers show the typical cuboidal morphology (Fig. 7). TEM images of A549 cells put in contact with all the fibres show evidence of cell damage, such as loss of cytoplasmic organelles and superficial protrusions. In addition, as shown in cells put in contact

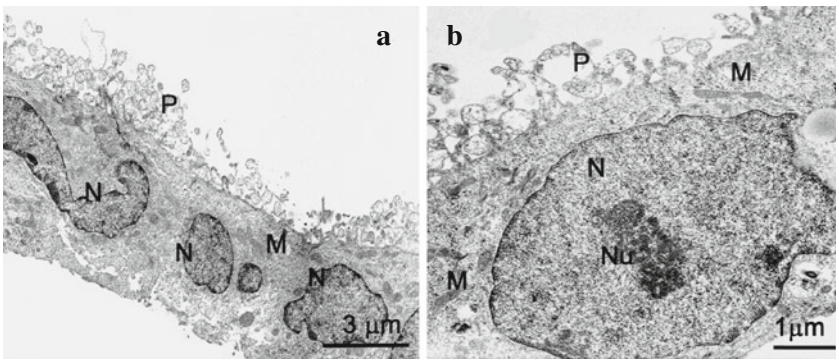

Fig. 7 TEM image of A549 control cells at 24 h: (**a**) cells with the typical cuboidal morphology; (**b**) higher magnification of the same cultured cells showing richness of peripheral cell protrusions and organelles. *N* nucleus, *Nu* nucleolus, *P* cell protrusions, *M* mitochondria

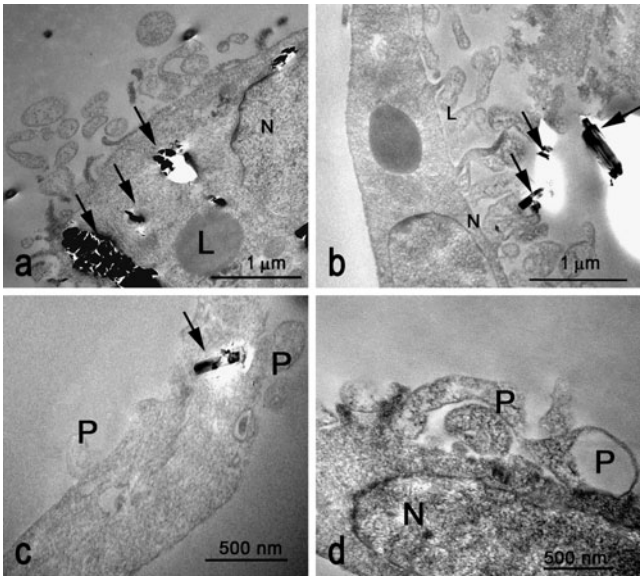

Fig. 8 TEM image of A549 cells at 24-h treated with 50 μg/ml of Ala di Stura tremolite: (**a**) tremolite asbestos aggregates (*black arrows*) inside cytoplasmic vacuoles and lipid droplets can be observed; (**b**) tremolite fibers (*black arrow*) outside a severely damaged cell with loss of protrusions; (**c**) tremolite fiber inside a cell with compromised cytoplasmic protrusions and aspects of severe damage; and (**d**) morphology of compromised cell with irregularly shaped protrusions and poorness of organules. *N* nucleus, *L* lipid droplet, *P* cytoplasmic protrusions

with Ala di Stura tremolite (Fig. 8), phagocytized minerals with the typical asbestiform habit are clearly observed inside cytoplasmic vacuoles. Notably, the cell internalization of fibers is observed to be independent of the fiber size.

It is already established that asbestos involves mitochondrial ROS production and induces apoptosis of the endothelial cells via the mitochondria-regulated (intrinsic) death pathway [53]. In the present study, results of MTT assay (Fig. 9) show significant decrements of cell viability with respect to the control cells for all asbestos-treated cells, except for Mt. Rufeno tremolite. This result indicates

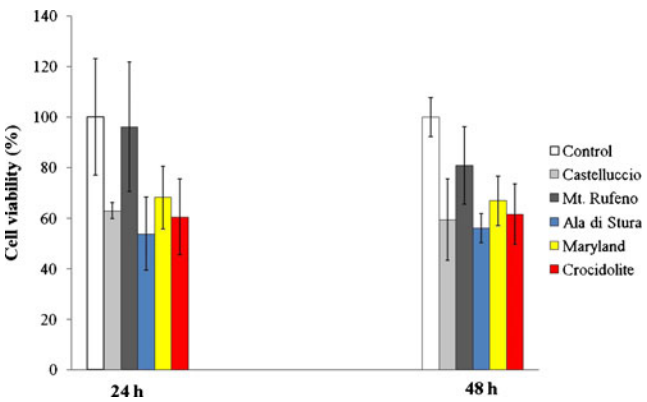

Fig. 9 MTT assay in A 549 cells. Comparison between treated and control cells at 24 and 48 h. *Error bars*, ±2 SD. Amphibole fibrous samples are ranked based on increasing Fe content

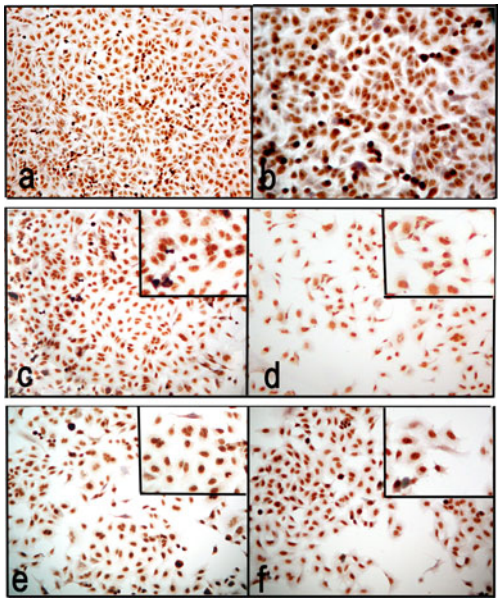

Fig. 10 Immunohistochemical Ki-67 detection at 48 h on A549 cells. Control cells: (**a**, **b**) cells treated with: (**c**) Mt. Rufeno tremolite, (**d**) Ala di Stura tremolite; (**e**) Castelluccio Superiore tremolite; (**f**) UICC crocidolite. Magnification: (**a**) ×200, (**b**) ×400, and (**c**–**f**) ×200 (with inserts, ×400)

the capability of the fibrous samples here tested to induce a suppression of mitochondrial functionality in different extent, as by MTT assay the mitochondrial succinate dehydrogenase enzyme is tested. In particular, Ala di Stura tremolite results to be even more toxic than UICC crocidolite. This result is not easily explainable as the toxic action of our samples could be related to many factors such as: the different capacity of fiber uptake that can affect cytoplasmic organelles; the release of Mg^{2+} that can have different effects on lipid packing, membrane permeability and can counteract Ca^{2+} uptake by blocking the calcium uniporter [12]; the release of Ca^{2+} that can affect the dysregulation of mitochondrial Ca^{2+} homeostasis leading to

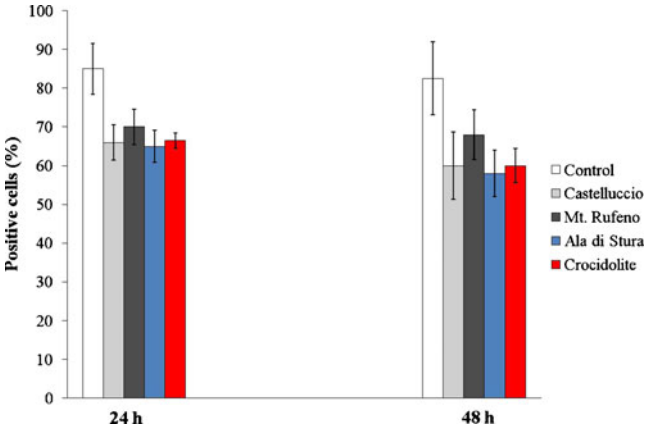

Fig. 11 Percent expression of Ki-67 antigen. *Error bars*, ±2 SD. Amphibole fibrous samples are ranked based on increasing Fe content

enhanced generation of ROS and induction of the permeability transition pore [12, 54].

Immunohistochemical Ki-67 detection shows marked decrements in proliferation of fiber-treated cells compared to control cultures for all tested samples (Fig. 10). The observed decline in the proliferation index seen in the asbestos-treated cells can be explained by the direct cytotoxic action of the fibers, and is in agreement with previous studies [55, 56]. The intensity of Ki-67 protein was evaluated with a number of positive cells: no significant differences are observed among the samples (Fig. 11).

Evidence of cellular stress in the asbestos-treated cells was also obtained with the analysis of pycnotic nuclei by fluorescence microscopy. After 24 h pycnotic nuclei are mostly detectable in cells treated with Ala di Stura and Maryland tremolites (Fig. 12a). In the same specimens, a decreased number of adherent cells was observed at 48 h (Fig. 12b), which may be due to the detachment of dead cells.

Except for cells in contact with Mt. Rufeno tremolite, hypodiploid peaks are generally observed, with strongest evidence for cells treated with Ala di Stura and Maryland tremolites (Fig. 12c). In addition, cytofluorimetric cell cycle analysis was also performed. Flow cytometry determines the relative cellular DNA content and enables the identification of the cell distribution during the various phases of the cell cycle. Four distinct phases could be recognized in a proliferating cell population: the G1-, S- (DNA synthesis phase), G2-, and M-phase (mitosis). G1 is the growth phase marked by synthesis of various enzymes, mainly those needed for DNA replication that are required in *S*-phase. During S phase, the amount of DNA in the cell is effectively doubled. G_2 phase is a period of rapid cell growth and protein synthesis during which the cell readies itself for mitosis.

Cells treated with Ala di Stura and Maryland tremolites show a G1 cycle phase strongly depressed with respect to control, whereas no significant difference between control and asbestos-treated cells may be observed for S and G2

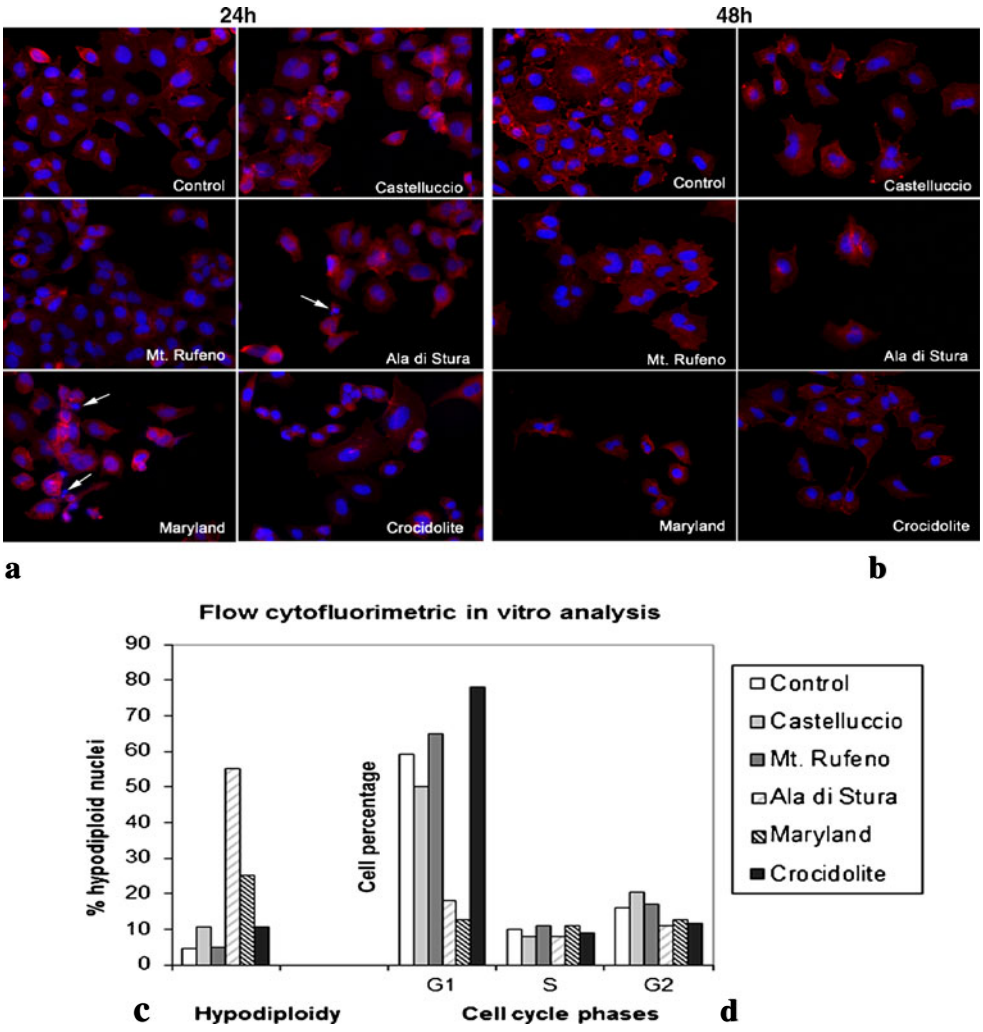

Fig. 12 Analysis of picnotic nuclei (↑) by fluorescence microscopy at: (**a**) 24 and (**b**) 48 h. Evaluation of hypodiploid nuclei (**c**) and cell cycle phases (**d**) by FACS analysis. Standard deviations are not shown because they are relative to mean values obtained from two experiments. Amphibole fibrous samples are ranked based on increasing Fe content

cycle phases (Fig. 12d). In particular, exposure of A549 cells to Ala di Stura and Maryland tremolite fibers cause a perturbation in the cells passing through the cell cycle, with a decrease in the number of cells in the G1 phase. These changes were concomitant with an increase in the number of cells containing hypodiploid nuclei. A G1 block was evidenced by the reduced number of cells entering S phase and the subsequent drop of cells in G2 phase (Fig. 12d).

Summarizing, results obtained from in vitro tests highlight that all tested samples, with the only exception of Mt. Rufeno tremolite, are responsible for significant cell toxicity. However, the toxicity of tremolite samples results to be not markedly different from that of UICC crocidolite. Notably, for specific tests (MTT and evaluation of hypodiploid nuclei) Ala di Stura tremolite is found to be even more cytotoxic than UICC crocidolite.

Conclusions

UICC crocidolite contains the highest quantity of Fe and exhibits the highest chemical reactivity; tremolite samples contain 10 to 20 times less Fe and show fairly lower chemical reactivity (Figs. 2, 3, 4, and 5). Moreover, the presence of Fe^{2+} and Fe^{3+} at the exposed M(1) and M(2) sites of the amphibole structure is a key factor of Fe availability for biochemical reactions (e.g., Fenton reaction). On these bases, a direct correlation between Fe topochemistry and fiber chemical reactivity is established. Relationship between crystal-chemical features and in vitro cell toxicity is not found to be so straightforward: UICC crocidolite has Fe content and chemical reactivity largely higher than that of tremolite samples, but all samples have comparable in vitro toxic potential. This is an independent confirmation that cell toxicity is due to the synergy of a number of processes and is still an entangled matter. Focusing on Fe topochemistry, it should be strongly related to cell genotoxicity better than cytotoxicity, because it plays a central role in the generation of HO· and production of MDA, with this latter well known to be highly carcinogenic [51, 52].

References

1. U.S. National Research Council (1985) Asbestiform fibres: non-occupational health risks. National Academy Press, Washington
2. Van Oss CJ, Naim JO, Costanzo PM Jr, Giese RF, Wu W, Sorling AF (1999) Impact of different asbestos species and other mineral particles on pulmonary pathogenesis. Clay Clay Min 47:697–707
3. Taunton AE, Druschel GK, Gunter ME, Wood SA (2010) Geochemistry in the lung: reaction-path modeling and experimental examinations of rock-forming minerals under physiologic conditions. Am Min. doi:10.2138/am.2010.3434
4. Trubiani O, Salvolini E, Staffolani R, Di Primio R, Mazzanti L (2003) DMSO modifies structural and functional properties of RPMI-8402 cells by promoting programmed cell death. Int J Immunopathol Pharmacol 16:253–259
5. Cardile V, Lombardo L, Belluso E, Panico A, Capella S, Balazy M (2007) Toxicity and carcinogenicity mechanisms of fibrous antigorite. Int J Environ Res Public Health 4:1–9
6. Elias Z, Poirot O, Schneider O, Amarande A-M, Danière M-C, Terzetti F, Pezerat H, Fournier J, Zalma R (1995) Cytotoxic and transforming effects of some iron-containing minerals in Syrian hamster embryo (SHE) cells. Cancer Detect Prev 19:405–414
7. Fubini B, Otero Arean C (1999) Chemical aspects of the toxicity of invale mineral dusts. Chem Soc Rev 28:373–381
8. Kamp DW, Weitzman SA (1999) The molecular basis of asbestos induced lung injury. Thorax 54:638–652
9. Shukla A, Gulumian M, Hei TK, Kamp D, Rahman Q, Mossman BT (2003) Serial review: role of reactive oxygen and nitrogen species (ROS/RNS) in lung injury and diseases. Multiple roles of oxidants in the pathogenesis of asbestos-induced diseases. Free Rad Biol Med 34:1117–1129
10. Kusmartsev S, Gabrilovich DI (2003) Inhibition of myeloid cell differentiation in cancer: the role of reactive oxygen species. J Leuk Biol 74:186–196
11. Halliwell B, Gutteridge JMC (1986) Oxygen free radicals and iron in relation to biology and medicine: some problems and concepts. Arch Biochem Biophys 246:501–514
12. Bergamini C, Fato R, Biagini G, Pugnaloni A, Giantomassi F, Foresti E, Lesci GI, Roveri N, Lenaz G (2007) Mitochondria changes induced by natural and synthetic asbestos fibers: studies on isolated mitochondria. Cell Mol Biol 52(Suppl):691–700
13. Panduri V, Surapureddi S, Soberanes S, Weitzman SA, Chandel N, Kamp DW (2006) P53 mediates amosite asbestos-induced alveolar epithelial cell mitochondria-regulated apoptosis. Am J Respir Cell Mol Biol 34:443–452
14. Pezerat H, Zalma R, Guignard J, Jaurand M-C (1989) Production of oxygen radicals by the reduction of oxygen arising from the surface activity of mineral fibres. In: Saracci R (ed) Non-occupational exposure to mineral fibers, vol 90. IARC Scientific Publication, Lyon, pp 100–110
15. Zalma R, Bonneau L, Guignard J, Pezerat H, Jaurand M-C (1987) Production of hydroxyl radicals by iron solid compounds. Toxicol Environ Chem 13:171–187
16. Fubini B, Fenoglio I, Elias Z, Poirot O (2001) On the variability of the biological responses to silicas: effect of origin, crystallinity and state of the surface on the generation of reactive oxygen species and consequent morphological transformations in cells. J Environ Pathol Toxicol Oncol 20:87–100
17. Gazzano E, Riganti C, Tomatis M, Turci F, Bosia A, Fubini B, Ghigo D (2005) Potential toxicity of nonregulated asbestiform minerals: balangeroite from the western Alps. Part 3: depletion of antioxidant defenses. J Toxicol Environ Health 68:41–49
18. Fournier J, Guignard J, Nejjari A, Zalma R, Pezerat H (1991) In: Brown RC (ed) The role of iron in the redox surface activity of fibers. Relation to carcinogenicity, mechanisms in fibre carcinogenesis. Plenum Press, New York, pp 407–414
19. Fournier J, Copin E, Dwigaj S, Chouchane S, Guignard J (1995) Peroxidation lipidique en présence de composés inorganiques. Relation avec les mécanismes du stress oxydant. C R Soc Biol 189:1–15
20. Chouchane S, Guignard J, Fournier J (2000) Lipid peroxidation in the presence of iron oxides. Toxicol Environ Chem 75:43–57
21. Wagner JC, Sleggs CA, Marchand P (1960) Diffuse pleural mesothelioma and asbestos exposure in the Northwestern Cape Province. Br J Ind Med 17:260–271
22. Ross M, Nolan RP (2003) History of asbestos discovery and use and asbestos-related disease in context with the occurrence of

asbestos within ophiolite complexes. Geol Soc Am Special Paper 373, Bpulder
23. Ballirano P, Andreozzi GB, Belardi G (2008) Crystal chemical and structural characterization of fibrous tremolite from Susa Valley, Italy, with comments on potential harmful effects on human health. Am Min 93:1349–1355
24. Pacella A, Andreozzi GB, Ballirano P, Gianfagna A (2008) Crystal chemical and structural characterization of fibrous tremolite from Ala di Stura (Lanzo Valley, Italy). Per Min 77:51–62
25. Davis JMG, Addison J, McIntosh C, Miller BG, Niven K (1991) Variations in the carcinogeneticy of tremolite dust samples of differing morphology. Ann N Y Acad Sci 643:473–490
26. Addison J, McConnel EE (2005) A review of carcinogenicity studies of asbestos and non-asbestos tremolite and other amphiboles. In: International symposium on the health hazard evaluation of fibrous particles associated with taconite and the adjacent duluth complex, St. Paul
27. Burragato F, Ballirano P, Fiori S, Papacchini L, Sonno M (2001) Segnalazione di tremolite asbestiforme nel Lazio. Il Cercapietre, vol. I–II, Notiziario del Gruppo Mineralogico Romano, pp 33–35
28. Punturo R, Fiannacca P, Lo Giudice A, Pezzino A, Cirrincione R, Liberi F, Piluso E (2004) Le Cave storiche della "Pietra Verde" di Gimigliano e Monte Reventino (Calabria): studio petrografico e geochimico. Acc Gioen Sci Nat Catania 37:35–57
29. Pasetto R, Bruni BM, D'Antona C, De Nardo P, Di Maria G, Di Stefano R, Fiorentini C, Gianfagna A, Marconi A, Paoletti L, Putzu MG, Soffritti M, Comba P (2004) Problematiche sanitarie della fibra anfibolica di Biancavilla. Aspetti epidemiologici, clinici e sperimentali. Note dell' Istituto Superiore di Sanità 17: 8–12
30. Pacella A, Andreozzi GB, Fournier J (2010) Detailed crystal chemistry and iron topochemistry of asbestos occurring in its natural setting: a first step to understanding its chemical reactivity. Chem Geol 277:197–206
31. Gavino VC, Miller JS, Ikharebha SO, Milo GE, Corwell DG (1981) Effect of polyunsaturated fatty acids and autoxidation on lipid peroxidation in tissue culture. J Lipid Res 22:763–769
32. Marcuse R, Johansson L (1973) Studies on the TBA test for rancidity grading: II. TBA reactivity of aldehyde classes. J Am Oil Chem Soc 50:387–391
33. Adiseshaiah P, Lindner DJ, Kalvakolanu DV, Reddy SP (2007) FRA-1 proto-oncogene induces lung epithelial cell invasion and anchorage-independent growth in vitro, but is insufficient to promote growth in vivo. Cancer Res 67:6204–6211
34. Pugnaloni A, Lucarini G, Giantomassi F, Lombardo L, Capella S, Belluso E, Zizzi A, Panico AM, Biagini G, Cardile V (2007) In vitro study of biofunctional indicators after exposure to asbestos-like fluoro-edenite fibres. Cell Mol Biol 53:965–980
35. Mossman BT (1983) Rapid colorimetric assay for cellular growth and survival: application to proliferation and cytotoxicity assays. J Immunol Methods 65:55–63
36. Gasparini G, Boracchi P, Verderio P, Bevilacqua P (1994) Cell kinetics in human breast cancer: comparison between the prognostic value of the cytofluorimetric S-phase fraction and that of the antibodies to Ki-67 and PCNA antigens detected by immunocytochemistry. Int J Cancer 57:822–829
37. Vielh P, Chevillard S, Mosseri V, Donatini B, Magdelenat H (1990) Ki67 index and S-phase fraction in human breast carcinomas. Comparison and correlations with prognostic factors. Am J Clin Pathol 94:681–686
38. Healy E, Angus B, Lawrence CM, Rees JL (1995) Prognostic value of Ki67 antigen expression in basal cell carcinomas. Br J Dermatol 133:737–741
39. Uboldi C, Bonacchi D, Lorenzi G, Hermanns MI, Pohl C, Baldi G, Unger RE, Kirkpatrick CJ (2009) Gold nanoparticles induce cytotoxicity in the alveolar type-II cell lines A549 and NCIH441. Part Fibre Toxicol 6:18
40. Telford WG, King LE, Fraker PJ (1992) Comparative evaluation of several DNA binding dyes in the detection of apoptosis associated chromatin degradation by flow cytometry. Cytometry 13:137–143
41. Leake BE, Woolley AR, Birch WD, Burke EAJ, Ferraris G, Grice JD, Hawthorne FC, Kisch HJ, Krivovichev VG, Schumacher JC, Stephenson NN, Withtaker EJW (2003) Nomenclature of amphiboles: additions and revisions to the International Mineralogical Association's amphibole nomenclature. Can Min 41:1355–1370
42. Bowes DR, Farrow CM (1997) Major and trace element compositions of the UICC standard asbestos sample. Am J Ind Med 32:592–594
43. Fubini B, Mollo L (1995) Role of iron oxides. Toxicol Lett 82/ 83:951–960
44. Wylie AG (1979) Optical properties of the fibrous amphiboles. Ann N Y Acad Sci 330:600–605
45. Verkouteren JR, Wylie AG (2002) Anomalous optical properties of fibrous tremolite, actinolite, and ferro-actinolite. Am Min 87:1090–1095
46. Fantauzzi M, Pacella A, Atzei D, Gianfagna A, Andreozzi GB, Rossi A (2010) Combined use of X-ray photoelectron and Mössbauer spectroscopic techniques in the analytical characterization of iron oxidation state in amphibole asbestos. Anal Bioanal Chem 396:2889–2898
47. Pezerat H, Zalma R, Guignard J (1989) Production of oxygen free radicals by the reduction of oxygen arising from the surface activity of mineral fibres. IARC Spl Publ 90:100–111
48. Bignon J, Peto J, Saracci R (1989) Non-occupational exposure to mineral fibres. Oxford University Press, Oxford
49. Marnett LJ (1999) Chemistry and biology of DNA damage by malondialdehyde, [Review]. IARC Sci Publ (150):17–27
50. Zhang Y, Chen S, Hsu T, Santella RM (2002) Immunohistochemical detection of malondialdehyde–DNA adducts in human oral mucosa cells. Carcinogenesis 23:207–211
51. Chouchane S, Guignard J, Fournier J (1999) Lipid peroxidation in presence of iron oxides. Toxicol Environ Chem 75:43–57
52. Nejjari A, Fournier J, Pezerat H, Leanderson P (1993) Mineral fibres: correlation between oxidising surface activity and DNA base hydroxylation. Occup Environ Med 50:501–504
53. Liu G, Beri R, Mueller A, Kamp DW (2010) Molecular mechanisms of asbestos-induced lung epithelial cell apoptosis. Chem Biol Interact 188(2):309–318
54. Shukla A, Ramos-Nino M, Mossman B (2003) Cell signaling and transcription factor activation by asbestos in lung injury and disease. Int J Biochem Cell Biol 35:1198–1209
55. Zheng N, Sun YF, Pei DS, Liu JJ, Sun XQ, Chen JC, Cai WQ, Li W, Cao JY (2005) Anti-Ki-67 peptide nucleic acid affects the proliferation and apoptosis of human renal carcinoma cells in vitro. Life Sci 76:1873–1881
56. Giantomassi F, Gualtieri AF, Santarelli L, Tomasetti M, Lusvardi G, Lucarini G, Governa M, Pugnaloni A (2010) Biological effects and comparative cytotoxicity of thermal transformed asbestos-containing materials in a human alveolar epithelial cell line. Toxicol In Vitro 24:1521–1531